ARTICLE

Template-Free Synthesis of Mesoporous CuO Dandelion Structures For Optoelectronic Applications

Sujit Manna, Kajari Das, and S. K. De*

Department of Material Science, Indian Association for the Cultivation of Science, Jadavpur, Kolkata 700 032, India

ABSTRACT A simple template-free hydrothermal route was used for the synthesis of novel mesoporous CuO dandelion structures formed by self-organized CuO nanorods. A very high surface area ~325 m^2/g and remarkably enhanced photoconductivity under white light irradiation of the CuO dandelions were observed compared to the nanocrystals. The extremely high photoconductivity is attributed to the presence of oxygen related hole-trap states at the large surface area of the dandelions. The fast response ($\tau = 24$ s) of the photocurrent holds promise for the fast photo-sensing device applications.

KEYWORDS: dandelions • self assembled • mesoporous • BET surface area • photo response • recombination

1. INTRODUCTION

Mesoporous materials have attracted widespread attention in different areas of science and industry, such as catalysis, adsorption, biomolecular separation, drug delivery, etc. (1−4). Nanostructures have some unique properties because of their inherent large surface-to-volume ratio and quantum size effects, which differ from those of the corresponding bulk materials (5). Self-assembly of these nanostructures into a mesoporous material with multiscale structures is of remarkable significance because of their unique properties associated with the nanostructures. Moreover, the optical and electronic properties of these mesoporous materials are strongly influenced by their high specific surface areas, uniform systems of pores, and crystalline pore walls at nanoscale dimension (6, 7).

Among all the metal oxides, cupric oxide (CuO) is one of the most studied materials in the literature because of its potential in various fields of application. As a p-type semiconductor with a narrow band gap of $E_g = 1.2$ eV, CuO is a potential field emitting material, an important catalyst, and a good gas sensor (8−10). CuO-based materials are well-known with regard to their giant magnetoresistance and high-temperature superconductivity (11, 12). It is also a promising material for fabricating optical switches and solar cells because of its photoconductive and photochemical properties (13−15). Moreover, the low band gap of CuO could prove it useful in photo detection and optical switching applications in the visible range where other metal oxides with their larger band gaps fail to perform (16).

Till now, a number of methods are known to synthesize CuO nanostructures with different morphologies, such as nanoparticles, nanorods, nanowires, nanotubes, nanoribbons, and peanutlike patterns (17−22), but very few reports of synthesis of mesoporous structures exist. Introduction of mesoporosity could drastically enhance the surface properties of CuO material and this area is still almost unexplored. Generally, mesoporous metal oxides are synthesized by neutral templating and ligand-assisted templating methods (23, 24). In our present work, a very simple template-free hydrothermal route was used to synthesize mesoporous CuO dandelion structures. H. C. Zeng reported the more complex solvothermal synthesis route and growth mechanism of the porous CuO dandelions formed by the mesoscale organization of CuO nanoribbons (25). G. Shi and his collaborators prepared the nanoporous CuO film using 3D dandelions and 2D Nanowalls of Copper Phosphate Dihydrate on a Copper Surface (26). Z. Jia et al. measured the BET surface area ~295 m^2/g of the porous CuO using Nitrogen-sorption studies, which is lower than the BET surface area of our sample porous CuO dandelions (27). To the best of our knowledge, the high porosity and photoconductivity of the porous CuO dandelion structures with mesoscale organization of nanorods have not yet been studied.

2. EXPERIMENTAL SECTION

A simple hydrothermal method was used to synthesize phase pure CuO dandelion structures. In a typical procedure, 10 mM cupric acetate monohydrate [$Cu(CH_3COO)_2.H_2O$] and 12.5 mM NaOH were mixed with 18 mL of deionized water (pH of the experimental solution ~6.5) under constant magnetic stirring for 1 h. The mixer was then transferred to a Teflon-lined stainless steel autoclave with 23 mL capacity and heat treated at the temperature 140 °C for 12 h. The autoclave chamber was air-cooled to room temperature after the reaction. The resulting precipitate was recovered by centrifugation and washed several times with deionized water and ethanol, and the precipitate was finally vacuum dried at 60 °C for 24 h. To understand the growth mechanism of the CuO dandelions, we also collected the intermediate products without heat treatment and heat treated at 140 °C for 1, 3 and 6 h.

To understand the photoresponse improvement of the synthesized product compared to the nonporous nanocrystals,

* Corresponding author. Tel.: +91-33-2473-3073. Fax: +91-33-2473-2805. E-mail: msskd@iacs.res.in.

Received for review March 9, 2010 and accepted April 20, 2010

DOI: 10.1021/am100197w

Published on Web 05/03/2010

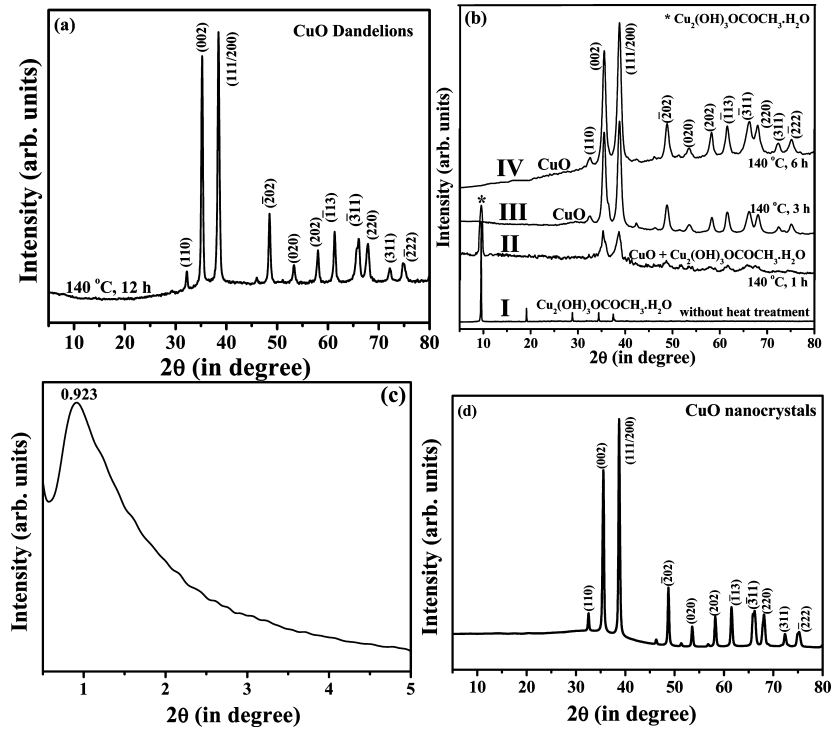

FIGURE 1. XRD patterns of the (a) CuO dandelion sample prepared at 140 °C for 12 h and (b) four intermediate products prepared at room temperature (I), 140 °C for 1 h (II), 140 °C for 3 h (III), and 140 °C for 6 h (IV), respectively. (c) Small-angle powder X-ray diffraction pattern of the CuO dandelion sample prepared at 140 °C for 12 h. (d) XRD pattern of the CuO nanocrystal sample.

another sample was prepared using copper nitrate [$Cu(NO_3)_2 \cdot 3H_2O$] instead of cupric acetate monohydrate. NaOH was taken to be 1.25 mM and all other experimental conditions were kept constant. The product was denoted by CuO nanocrystals.

The crystalline phases of the products were determined by X-ray powder diffraction by using a Bruker AXS D8 SWAX diffractometer with Cu K_α radiation ($\lambda = 1.54$ Å). The morphologies of the samples were studied by a field emission scanning electron microscope (FESEM, JEOL, JSM- 6700F). Microstructural properties were obtained using transmission electron microscope (TEM, JEOL 2010). For the TEM observations, the powders were dispersed in 2-propanol and ultrasonicated for 15 min. A few drops of this ultrasonicated solution were taken on a carbon coated copper grid. Nitrogen adsorption/desorption isotherms were obtained using a Bel Japan Inc. Belsorp-HP at 77 K.

For electrical characterization, the sample was deposited on glass substrates through spin-casting. First the powder sample dispersed in methanol (2 mg/mL) was spun at a speed of 1000 rpm resulting in a thin film of CuO. The films were dried in vacuum at 60 °C for 12 h. For the photo response measurements, two gold electrodes (of 50 nm thickness) were thermally evaporated on the film surface in the circular form of diameter 1 mm through a shadow mask at a separation of 3 mm. The photocurrents were measured by illuminating the sample with white light from a He−Cd laser (Kimmon Koha Co., Ltd., model KR1801C) of 100 mW power and 3 V biasing condition using the Keithley picoammeter (model 2400). All of the experiments were done in ambient air at room temperature.

3. RESULTS AND DISCUSSION

Figure 1a shows the X-ray diffraction (XRD) pattern of the sample prepared at the reaction temperature 140 °C for 12 h, reveals that all the peaks correspond to the reflections from (110), (002), (111/200), ($\bar{2}$02), (020), (202), ($\bar{1}$13), ($\bar{3}$11), (220), (311) and ($\bar{2}$22) planes of monoclinic cupric oxide (CuO), which are consistent with the standard reported values (JCPDS File no. 41−0254). Figure 1b shows the XRD patterns of all the intermediate products collected without heat treatment and heat treated for 1, 3, and 6 h. The XRD pattern I of the product without heat treatment reveals that the reaction of the $Cu(CH_3COO)_2 \cdot H_2O$ with NaOH aqueous solution (OH^-/Cu^{2+} ratio ~1) gives monoclinic copper hydroxide acetate [$Cu_2(OH)_3OCOCH_3 \cdot H_2O$] under constant stirring for 1 h (28). After 1 h heat treatment at 140 °C, a mixture of CuO and $Cu_2(OH)_3OCOCH_3 \cdot H_2O$ was found (XRD pattern II). The pure phase CuO (XRD pattern III) was obtained when the reaction time was 3 h. The XRD pattern IV of the sample at reaction time 6 h also gives the pure phase CuO. To obtain the well-crystalline spherical product, we carried out the final reaction for 12 h. The FWHM values of the (111) peak for the three pure phase samples at 3, 6, and 12 h were measured ~0.89, 0.67, and 0.46 respectively, reveals that the crystallinity of the sample increases with increasing the reaction time. Figure 1c gives the small-angle powder X-ray diffraction pattern of the final CuO sample. A single broad diffraction peak at low 2θ is observed, suggesting the disordered mesophases. No distinctive higher-order diffraction was observed for the sample. The *d*-spacing of mesostructure is 9.6 nm as calculated from the maxima of the XRD pattern. Figure 1d shows the XRD pattern of the sample obtained using copper nitrate [$Cu(NO_3)_2 \cdot 3H_2O$] at 140 °C for 12 h indicates pure phase CuO.

Figure 2a shows the spherical structures with diameters 1−2.5 μm of the final product obtained at 140 °C for 12 h. Interestingly, the CuO nanorods self-organized into spherical assemblies or "dandelion" structure, which is clearly

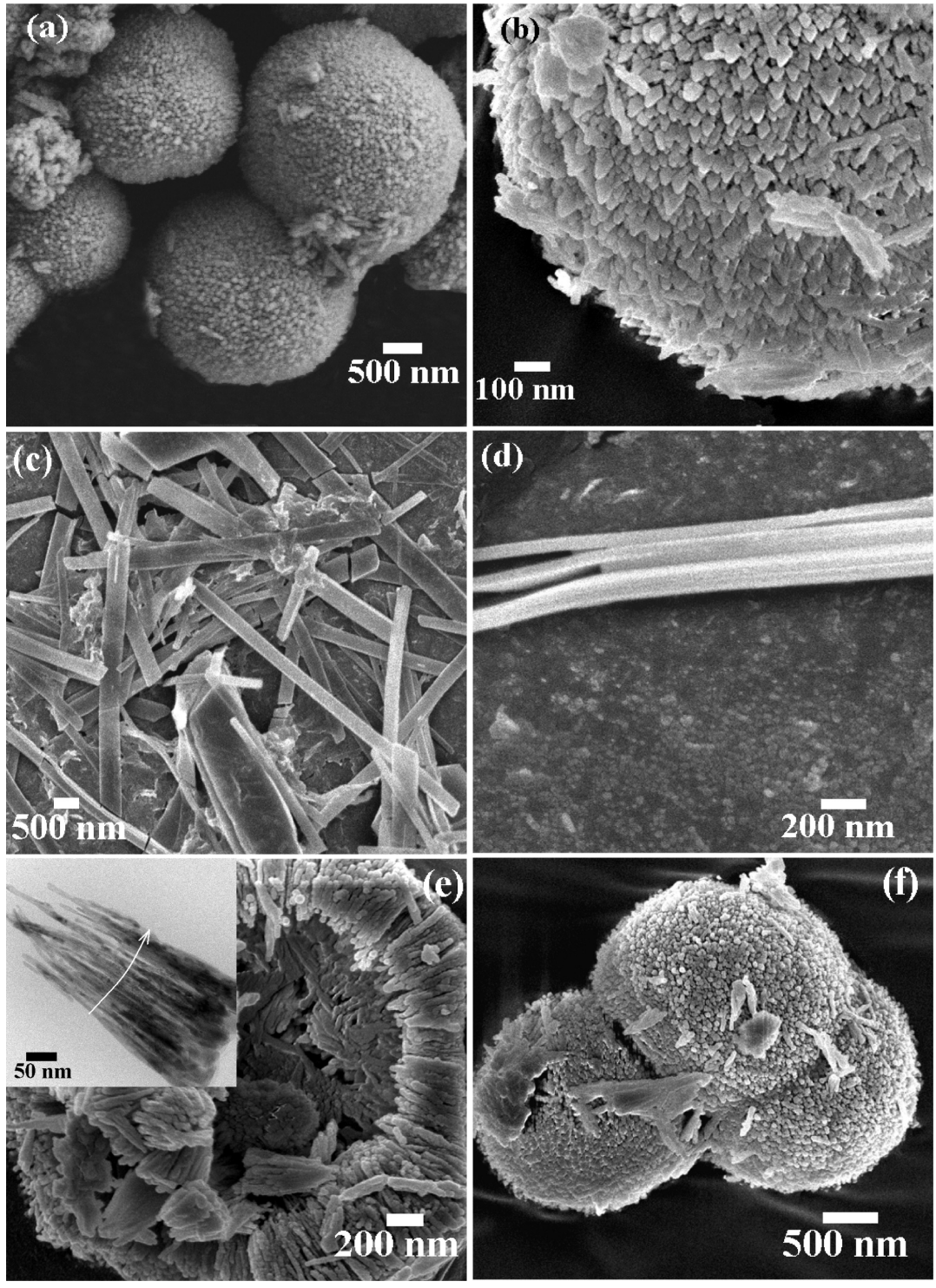

FIGURE 2. (a) Low-resolution and (b) high-resolution FESEM images of the CuO dandelion sample prepared at 140 °C for 12 h; FESEM images of the intermediate products prepared at (c) room temperature, (d) 140 °C for 1 h, (e) 140 °C for 3 h, and (f) 140 °C for 6 h, respectively. The inset of (e) shows the TEM image of the self-organization of nanorods.

shown in Figure 2b. Figure 2c–f shows the intermediate products for forming the dandelion structures at different time intervals. The constant magnetic stirring of the $Cu(CH_3COO)_2 \cdot H_2O$ in NaOH aqueous solution at room temperature formed the sheetlike nanostructures of breadth 400–800 nm and length several micrometers, shown in Figure 2c. The splitting of these nanosheets was observed after 1 h heat treatment at 140 °C. Figure 2d shows the one end splitted nanosheet. Figure 2e shows the FESEM image of the product obtained at 140 °C for 3 h, which reveals that the CuO dandelion structures were started to form by the self organization of the splitted nanosheets, i.e, irregular shaped nanorods of CuO. The TEM image shown in the inset of the Figure 2e clearly shows the self organization of the nanorods. After 6 h heat treatment, the complete dandelion structures were formed shown in the Figure 2f.

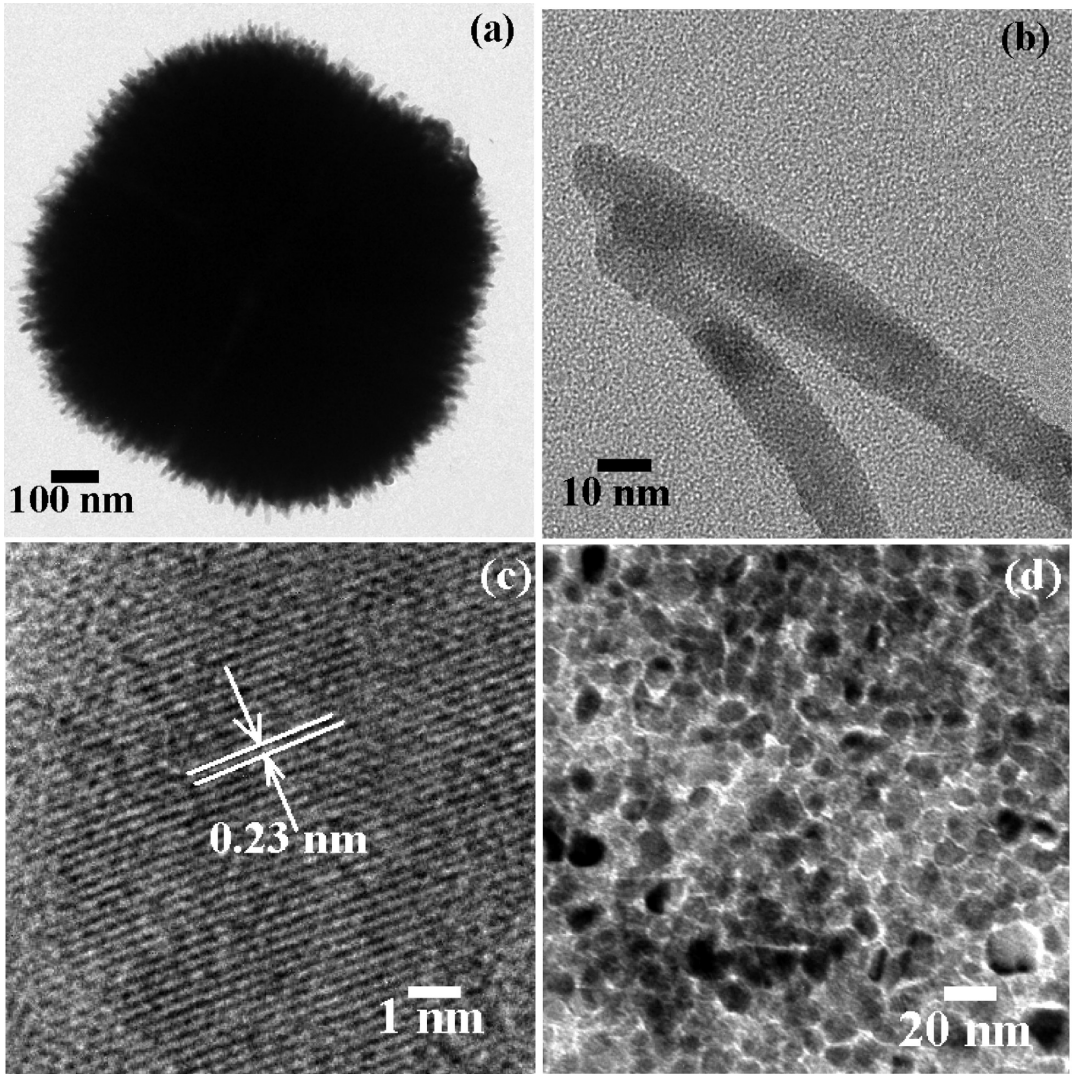

FIGURE 3. Low-resolution TEM images of (a) a single CuO dandelion and (b) the irregular-shaped CuO nanorods by which the dandelion structure was formed. (c) HRTEM image of a single CuO nanorod. (d) TEM image of the CuO nanocrystals sample.

Figure 3a shows the low-resolution TEM image of the CuO dandelion structure, which also reveals that the spherically self assembled of the CuO nanorods give the dandelion structure. Figure 3b shows the two irregularly shaped CuO nanorods of diameter ~11 nm, by which the dandelion structure was formed. The HRTEM image of a single nanorod shown in Figure 3c indicates 0.23 nm spacing between two adjacent lattice planes of a nanorod corresponding to the (111) lattice planes of CuO. The TEM image shown in Figure 3d indicates that the nanoparticles shaped CuO nanocrystals of average diameter ~12 nm were formed by the reaction of 10 mM $Cu(NO_3)_2 \cdot 3H_2O$ with 1.25 mM NaOH aqueous solution at 140 °C for 12 h.

By the aid of the XRD, FESEM, and TEM studies, the proposed growth mechanism of the dandelion structures were depicted. Figure 4 shows the schematic diagram of the growth process of the CuO dandelion structures. The constant magnetic stirring of the $Cu(CH_3COO)_2 \cdot H_2O$ with NaOH aqueous solution at room temperature gives $Cu_2(OH)_3$-$OCOCH_3.H_2O$ compound (XRD spectrum I of Figure 1b), which has a single-layered structure as shown in Figure 4 (29, 30). Therefore, the sheetlike morphologies were prima-

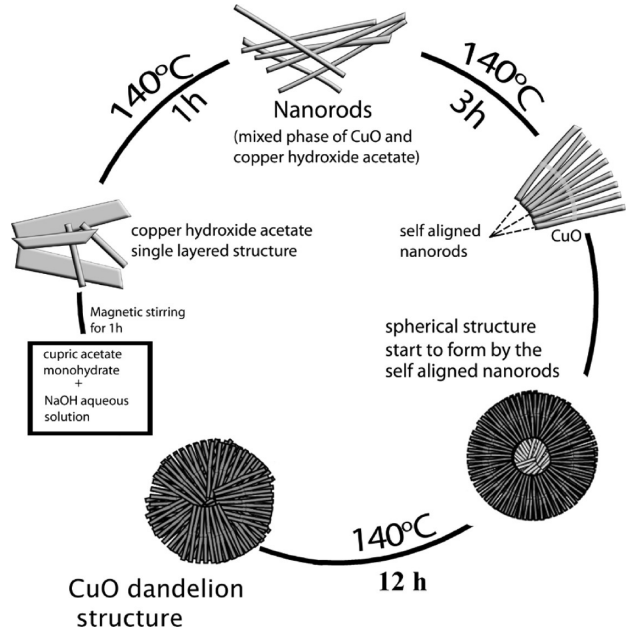

FIGURE 4. Schematic diagram for the growth mechanism of the CuO dandelion structures.

rily formed at room temperature, shown in the FESEM image of Figure 2c. On heating above 100 °C, $Cu_2(OH)_3OCOCH_3 \cdot H_2O$ compound losses the hydrated water (30). Therefore, the $Cu_2(OH)_3OCOCH_3.H_2O$ sheets were irregularly splitted after 1 h heating at 140 °C due to the losses of the water molecules and simultaneously transformed to the CuO phase as revealed by the XRD spectrum II of Figure 1b. The product obtained after 3 h of reaction was pure phase CuO (XRD spectrum III of Figure 1b). These splitted sheets, i.e., nanorods of irregular diameter of pure phase CuO, are aligned perpendicularly to the spherical surface, along main crystallographic axes of CuO, pointing toward a common center, via an "oriented attachment" process (The inset of the Figure 2e) (31−33). As the reaction progresses, the CuO nanorods were gradually organized into microspheres. The product obtained after 3 h of reaction (FESEM image Figure 2e) gives the incomplete puffy, porous microspheres formed by the oriented attachment of the CuO nanorods. After 6 h reaction, the formation of the dandelion structure like microspheres was completed (FESEM image Figure 2f). The reaction was carried out for 12 h to get the well crystalline porous pure phase CuO dandelions. Some template free synthesis processes of hierarchical nanostructured CuO were previously reported (34−36). J. P. Tu and his co-workers reported the self-assembled synthesis of hierarchical nanostructured CuO with various morphologies (35). In this case, the reaction of $Cu(CH_3COO)_2 \cdot H_2O$ with NH_3 solution at room temperature gives a $Cu(OH)_2$ nanowire precursor, by which the different hierarchical nanostructured CuO were formed at different pH values of ∼9.5−11.5. But in our case, the pH of the experimental solution was 6.5; the lower pH may be responsible for the formation of sheetlike $Cu_2(OH)_3OCOCH_3 \cdot H_2O$ compound. Singh et al. reported the synthesis of different CuO nanostructures using $Cu(NO_3)_2 \cdot 3H_2O$ with different molar concentrations of NaOH (34). The rectangular-shaped nanocrystals were formed when the molar ratio of OH^-/Cu^{2+} was 0.5. In our case, 1.25 mM NaOH aqueous solution was mixed with 10 mM $Cu(NO_3)_2 \cdot 3H_2O$ (molar ratio of OH^-/Cu^{2+} ∼0.125),which gives nanoparticle-shaped CuO nanocrystals, no 1D structure. Therefore, it may be concluded that the acetate group and lower pH of the experimental solution play important roles in the synthesis of mesoporous CuO dandelions, whereas the nitrate at lower NaOH concentration gives the CuO nanocrystals.

Figure 5a shows the N_2 adsorption/desorption isotherms of mesoporous CuO dandelion structures at 77 K. These isotherms could be classified as type IV with a steep rise due to capillary condensation, characteristic of mesoporous materials (37). The BET surface area was found to be 325 m^2/g. The inset of the Figure 5a gives the average pore diameter of the CuO dandelion structure ∼5.7 nm. The high-magnification TEM image shown in the inset of Figure 2e also confirms the presence of many disordered pores with sizes less than 5 nm in the dandelion structures. From the pore size distribution and low-angle XRD results, pore wall thickness was calculated using the formula $((2d)/(\sqrt{3}) -$ pore

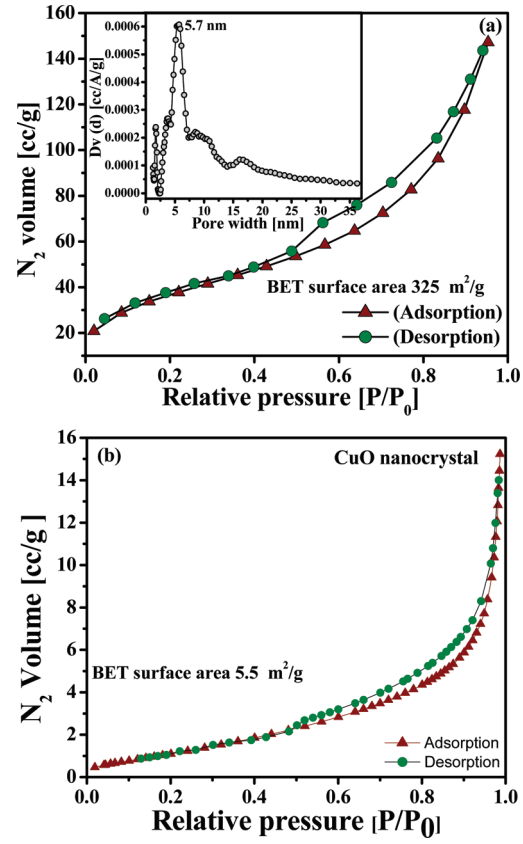

FIGURE 5. N_2 adsorption/desorption isotherms of (a) mesoporous CuO dandelion structures and (b) CuO nanocrystals at 77 K. The inset of figure a shows the NLDFT pore size distributions of CuO dandelion sample.

diameter) ≈ 5.3 nm, where d is the d-spacing of mesostructure calculated from the maxima of the low-angle XRD pattern. The nitrogen adsorption−desorption isotherms of the CuO dandelions also display a clear hysteresis loop (Figure 5a), which is characteristic of mesoporous 3D materials with cagelike or disordered pores (38−42). To the best of our knowledge, the mesoporous CuO dandelion structures reported herein are the first to show a classical type IV N_2 sorption isotherm, and have much higher specific surface area. To compare the porosity of the porous dandelions with the nonporous CuO nanocrystals, we also measured the N_2 adsorption/desorption isotherms of CuO nanocrystals at 77 K, shown in Figure 5b. The BET surface area of CuO nanocrystals was found to be 5.5 m^2/g. Thus it may be concluded that the porous CuO structures have larger surface area than the nonporous CuO nanocrystals.

The schematic diagram for the photocurrent measurements is shown in the inset of Figure 6a. To optimize the performance of the as-fabricated device, the contact properties were investigated. In our experiment, Au electrodes were used to study the electrical properties of the CuO dandelion structures and CuO nanocrystals sample. The corresponding current−voltage ($I-V$) curves of the two samples shown in Figure 6a give linear characteristics, which indicate that the Ohmic contacts were established between Au and CuO. In general, the contact properties depend on the difference of work functions between the metal used as electrodes and the semiconductor. When the work function of the contact

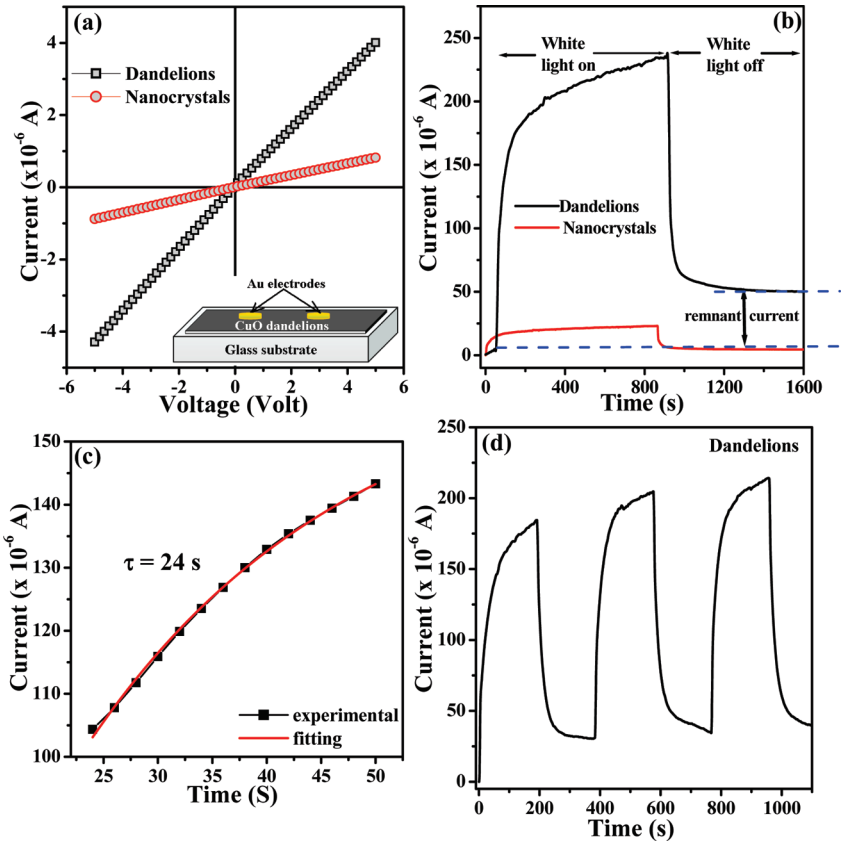

FIGURE 6. (a) Dark current−voltage ($I-V$) curves and (b) growth and decay curves of the photocurrent under and removal of 15 min white light illumination at 3 V bias voltage of the CuO dandelion structures and CuO nanocrystals sample; the inset of (a) is the schematic diagram of the photocurrent measurement device. (c) The experimental and fitted curves of the fast response region of photocurrent growth of the CuO dandelion structures. (d) Time-resolved measurement of photoresponse to white light of the CuO dandelion structures under the period of 3 min at 3 V bias voltage.

metal is larger than that of the semiconductor, an n-type semiconductor exhibits a Schottky barrier, whereas a p-type semiconductor exhibits Ohmic contact (43). The photocurrent growth and decay shown in Figure 6b were measured in ambient air by switching the white light "on" and "off" for 15 min each at 3 V bias. On white light illumination, the photocurrent in the CuO dandelion structures reaches a maximum value of 238 × 10^{-6} A, leading to the photo (I_{ph}) to dark current (I_d) ratio I_{ph}/I_d of 397, which is remarkably higher compared to the CuO nanocrystals ($I_{ph}/I_d \approx 92$). Therefore, the mesoporous dandelion structures show better sensitivity toward the white light than the CuO nanocrystals. As soon as the white light is switched off, the photocurrent drops very fast. Photogenerated carriers could significantly increase the conductivity when semiconductor materials are illuminated by white light. Meanwhile the large surface area (BET surface area ~325 m^2/g) of the mesoporous CuO dandelion structures is able to further enhance the sensitivity to white light and might even lead to the realization of single photon detection (44). The optical and electronic properties of materials mainly depend on the stoichiometry. It is generally accepted that CuO is metal deficient ($Cu_{1-\delta}O$) oxide material with a corresponding defect equation described as

$$\frac{1}{2}O_2 \leftrightarrow V_{Cu}^{2-} + 2h^+ + O_0 \qquad (1)$$

Where V_{Cu}^{2-} and h^+ represent the concentration of copper vacancies and holes, respectively. The existence of copper vacancies results in the production of holes and agrees with the p-type semiconducting behavior of CuO (45). It is well-known that the surface defects of metal oxides nanostructures function as O_2 adsorption sites in air because of the high availability of the surface area, previously shown in the case of ZnO nanorods and TiO_2 nanocrystalline films (46, 47). Moreover, the mesoporous structures having large surface area compared to the nonporous nanostructures may adsorb more O_2 molecules. According to the defect eq 1, it may also be suggested that the concentration of holes and thus the electrical carrier concentrations, i.e., the conductivity of CuO dandelions could be highly sensitive to the presence of absorbed O_2 molecules. In the dark, the O_2 molecules adsorbed on the CuO dandelion surfaces capture the minority charge carriers, i.e., electrons of the p-type CuO [O_2(gas) + $e^- \rightarrow O_2^-$(adsorbed)]. This electron transfer lowers of the quasi-Fermi level and increases the free hole density. As a result, the conductivity of the p-type CuO dandelions increase and a low-conducting depletion layer is formed near the surface. On illumination by the white light, the photogenerated and free holes of the p-type CuO drift to the surface along the potential slope produced by band bending and trapped by the adsorbed O_2^- through the surface electron-hole recombination [$h^+ + O_2^-$(adsorbed) → O_2(gas)]

and simultaneously the excess holes increase the conductivity of the CuO dandelions abruptly. Consequently, the unpaired electrons are either collected by the anode or recombine with holes generated when oxygen molecules are readsorbed and ionized at the surface of CuO dandelions. When the light is off, the electrons recombine with the holes and also are captured by the readsorbed O_2 molecules causing the increase of depletion width, which gives the faster decay in the current (48). Some remnant current was found to be present after sudden fall of the current (Figure 6b), which may result from the presence of the excess photogenerated holes in p-type CuO dandelions. The rising response of the photocurrent is clearly defined by two regions. The fast response region, which may be attributed to an intrinsic RC-circuit response, is fitted well with eq 2 using a nonlinear curve fitting program

$$I(t) = I_0(1 - e^{-t/\tau}) \quad (2)$$

where τ is the time constant. The experimental data and the corresponding fitted curves are shown in the Figure 6c. The time constant was found to be 24 s. The second region of the photo current growth curve, i.e., the slow rise region, may be due to the different processes involving surface-assisted carrier recombination, trapping, and defect-assisted recombination/generation within the CuO dandelions. Time-resolved measurement of photoresponse to white light was conducted and the result is shown in Figure 6d. The "on" current and "off" current for each of the three cycles remain the same within the noise envelope. The photoconductivity response time is three minutes. Therefore, the high photo to dark current ratio (∼397), rapid increase in the photocurrent under white light illumination, and the reversibility and stability of the photoresponse may make the CuO mesoporous dandelion structures applicable in solar cells and in optical switches.

4. CONCLUSION

In summary, a simple hydrothermal method was used to prepare porous CuO dandelion structures with mesoscale organization of nanorods. The plausible growth mechanism of the porous structures was predicted. The CuO dandelion structures depict a classical type IV N_2 sorption isotherm, which gives high BET surface area of ∼325 m^2/g. The photo (I_{ph}) to dark current (I_d) ratio I_{ph}/I_d of the mesoporous CuO dandelion structures is remarkably higher compared to the CuO nanocrystals. Therefore, exceptionally high specific surface area for this novel mesoporous CuO dandelion structures, along with drastic enhancement in photocurrent under white light irradiation, could lead to many potential applications, especially in optoelectronic devices such as optical switch, photo detector, solar cell, etc.

REFERENCES AND NOTES

(1) Fujiwara, M.; Terashima, S.; Endo, Y.; Shiokawa, K.; Ohue, H. *Chem. Commun.* **2006**, 4635–4637.
(2) Gierszal, K. P.; Jaroniec, M. *J. Phys. Chem. C* **2007**, *111*, 9742–9748.
(3) Fan, R.; Huh, S.; Yan, R.; Arnold, J.; Yang, P. *Nat. Mater.* **2008**, *7*, 303–307.
(4) Yang, P.; Quan, Z.; Li, C.; Lian, H.; Huang, S.; Lin, J. *Microporous Mesoporous Mater.* **2008**, *116*, 524–531.
(5) Kamat, P. V. *J. Phys. Chem. C* **2007**, *111*, 2834–2860.
(6) Yang, P.; Zhao, D.; Margolese, D. I.; Chmelka, B. F.; Stucky, G. D. *Nature* **1998**, *396*, 152–155.
(7) Brezesinski, T.; Erpen, C.; Iimura, K.-I.; Smarsly, B. *Chem. Mater.* **2005**, *17*, 1683–1690.
(8) Liu, Y.; Liao, L.; Li, J.; Pan, C. *J. Phys. Chem. C* **2007**, *111*, 5050–5056.
(9) Luo, M.-F.; Song, Y.-P.; Lu, J.-Q.; Wang, X.-Y.; Pu, Z.-Y. *J. Phys. Chem. C* **2007**, *111*, 12686–12692.
(10) Li, J.-Y.; Xiong, S.; Xi, B.; Li, X.-G.; Qian, Y.-T. *Cryst. Growth Des.* **2009**, *9*, 4108–4115.
(11) Lee, S. S.; Hwang, D. G.; Park, C. M.; Lee, K. A. *IEEE Trans. Magn.* **1997**, *33*, 3541–3549.
(12) MacDonald, A. H. *Nature* **2001**, *414*, 409–410.
(13) Ashida, M.; Ogasawara, T.; Tokura, Y.; Uchida, S.; Mazumdar, S.; Kuwata-Gonokami, M. *Appl. Phys. Lett.* **2001**, *78*, 2831–2833.
(14) Mittiga, A.; Salza, E.; Sarto, F.; Tucci, M.; Vasanthi, R. *Appl. Phys. Lett.* **2006**, *88*, 163502.
(15) Anandan, S. *Sol. Energy Mater. Sol. Cells* **2007**, *91*, 843–846.
(16) Kouklin, N. *Adv. Mater.* **2008**, *20*, 2190–2194.
(17) Zhou, K.; Wang, R.; Xu, B.; Li, Y. *Nanotechnology* **2006**, *17*, 3939–3943.
(18) Cao, M. H.; Hu, C. W.; Wang, Y. H.; Guo, Y. H.; Guo, C. X.; Wang, E. B. *Chem. Commun.* **2003**, 1884–1885.
(19) Jiang, X.; Herricks, T.; Xia, Y. *Nano Lett.* **2002**, *2*, 1333–1338.
(20) Cho, Y. S.; Huh, Y. D. *Bull. Korean Chem. Soc.* **2008**, *29*, 2525–2527.
(21) Wang, X.; Xi, G.; Xiong, S.; Liu, Y.; Xi, B.; Yu, W.; Qian, Y. *Cryst. Growth Des.* **2007**, *7*, 930–934.
(22) Zhang, L. Z.; Yu, J. C.; Xu, A. W.; Li, Q.; Kwong, K. W.; Yu, S. H. *J. Cryst. Growth* **2004**, *266*, 545–551.
(23) Zhang, H.; Wu, J.; Zhou, L.; Zhang, D.; Qi, L. *Langmuir* **2007**, *23*, 1107–1113.
(24) Yang, P.; Zhao, D.; Margolese, D. I.; Chmelka, B. F.; Stucky, G. D. *Chem. Mater.* **1999**, *11*, 2813–2826.
(25) Liu, B.; Zeng, H. C. *J. Am. Chem. Soc.* **2004**, *126*, 8124–8125.
(26) Wu, X.; Shi, G.; Wang, S.; Wu, P. *Eur. J. Inorg. Chem.* **2005**, 4775–4779.
(27) Jia, Z.; Yue, L.; Zheng, Y.; Xu, Z. *Mater. Res. Bull.* **2008**, *43*, 2434–2440.
(28) Masciocchi, N.; Corradi, E.; Sironi, A.; Moretti, G.; Minelli, G.; Porta, P. *J. Solid State Chem.* **1997**, *131*, 252–262.
(29) Kozai, N.; Mitamura, H.; Fukuyama, H.; Esaka, F. *J. Mater. Res.* **2005**, *20*, 2997–3003.
(30) Yamanaka, S.; Sako, T.; Hattori, M. *Chem. Lett.* **1989**, 1869–1872.
(31) Lou, X. W.; Zeng, H. C. *J. Am. Chem. Soc.* **2003**, *125*, 2697–2704.
(32) Liu, B.; Zeng, H. C. *J. Am. Chem. Soc.* **2003**, *125*, 4430–4431.
(33) Penn, R. L.; Banfield, J. F. *Science* **1998**, *281*, 969–971.
(34) Singh, D. P.; Ojha, A. K.; Srivastava, O. N. *J. Phys. Chem. C* **2009**, *113*, 3409.
(35) Xiang, J. Y.; Tu, J. P.; Zhang, L.; Zhou, Y.; Wang, X. L.; Shi, S. J. *J. Power Sources* **2010**, *195*, 313–319.
(36) Li, Y. G.; Tan, B.; Wu, Y. Y. *Chem. Mater.* **2008**, *20*, 567–576.
(37) Floquet, N.; Coulomb, J. P.; Weber, G.; Bertrand, O.; Bellat, J. P. *J. Phys. Chem. B* **2003**, *107*, 685–693.
(38) Wang, J.; Xia, Y.; Wang, W.; Mokaya, R.; Poliakoff, M. *Chem. Commun.* **2005**, 210–212.
(39) Wang, J.; Xia, Y.; Wang, W.; Poliakoff, M.; Mokaya, R. *J. Mater. Chem.* **2006**, *16*, 1751–1756.
(40) Kruk, M.; Jaroniec, M.; Sayari, A. *Langmuir* **1997**, *13*, 6267–6273.
(41) Kruk, M.; Jaroniec, M. *Chem. Mater.* **2001**, *13*, 3169–3183.
(42) Lee, B.; Lu, D.; Kondo, J. N.; Domen, K. *J. Am. Chem. Soc.* **2002**, *124*, 11256–11257.
(43) Sze, S. M. *Physics of Semiconductor Devices*; Wiley: New York, 1981.
(44) Hayden, O.; Agarwal, R.; Lieber, C. M. *Nature Mater.* **2006**, *5*, 352–356.
(45) Haugsrud, R. *J. Electrochem. Soc.* **2002**, *149*, B14–B21.
(46) Ahn, S. E.; Lee, J. S.; Kim, H.; Kim, S.; Kang, B. K.; Kim, K. H.; Kim, G. T. *Appl. Phys. Lett.* **2004**, *84*, 5022.
(47) Nelson, J.; Eppler, A. M.; Ballard, I. M. *J. Photochem. Photobiol., A* **2002**, *148*, 25–31.
(48) Soci, C.; Zhang, A.; Xiang, B.; Dayeh, S. A.; Aplin, D. P. R.; Park, J.; Bao, X. Y.; Lo, Y. H.; Wang, D. *Nano Lett.* **2007**, *7*, 1003–1009.

AM100197W